



Magnetism of crystalline and nanostructured ZnFe_2O_4

F.J. Burghart^a, W. Potzel^a, G.M. Kalvius^{a,*}, E. Schreier^a, G. Grosse^a, D.R. Noakes^b,
W. Schäfer^c, W. Kockelmann^c, S.J. Campbell^d, W.A. Kaczmarek^e, A. Martin^f,
M.K. Krause^g

^aPhysik-Department, Technische Universität München, E-15, James-Frank-Strasse, D-85747 Garching, Germany

^bPhysics Department, Virginia State University, Petersburg VA, 23806, USA

^cMineralogisch-Petrologisches Institut, Universität Bonn, D-53115 Bonn, Germany

^dSchool of Physics, University College, University of New South Wales, ADFA, Canberra ACT 2600, Australia

^ePhysical Sciences, The Australian National University, Canberra ACT 0200, Australia

^fChemisch-Geowissenschaftliche Fakultät, Universität Jena, D-07743 Jena, Germany

^gPhysik und Geowissenschaften, Universität Leipzig, D-04103 Leipzig, Germany

Abstract

We have investigated the magnetic properties of three differently prepared samples of the spinel ZnFe_2O_4 with μSR , neutron diffraction, Mössbauer effect and magnetization measurements. Below $T_N = 10.5$ K, the first sample (annealed) shows long-range antiferromagnetic order in coexistence with short-range magnetic order. The second sample (rapidly quenched) shows only short-range magnetic order. The third sample (nanostructured with an average particle size of about 9 nm) exhibits ferromagnetism below $T_c \approx 460$ K combined with superparamagnetism. Below the blocking temperature of ~ 50 K the nanostructured sample exhibits a dependence on applied magnetic fields similar to that observed in spin glass systems. The roles of cation-site occupation and magnetic couplings in governing the different magnetic behaviors exhibited by the samples are discussed. © 2000 Published by Elsevier Science B.V. All rights reserved.

PACS: 75.50.K; 75.50.G; 75.40.G

Keywords: Nanostructured magnet; Ferrite; Spin glass; Superparamagnetism

1. Introduction

The ferrite ZnFe_2O_4 is of interest not only to basic research in magnetism, but also has great potential in technological applications [1]. It crystallizes in the spinel structure which contains two different cation sites: eight tetrahedral A sites and 16 octahedral B sites. Magnetic coupling occurs via super exchange. The A–A and B–B couplings are

weak compared to the A–B interaction. In a *normal* spinel all Zn atoms are on A sites, all Fe atoms on B sites. In a fully *inverse* spinel the Zn atoms occupy half of the B sites, while half of the Fe atoms rest on A sites, the other half on B sites. Mixtures between the two configurations occur and are characterized by the ‘degree of inversion’ which depends strongly on the preparation procedures. In this paper we outline the influence of the degree of inversion on the magnetic properties of three different samples of ZnFe_2O_4 as investigated by μSR , neutron diffraction, ^{57}Fe Mössbauer effect and magnetization measurements.

* Corresponding author. Tel.: + 49-89-2891-2501; fax: + 49-89-320-6780.

E-mail address: kalvius@physik.tu-muenchen.de (G.M. Kalvius).

2. Experimental details

All three ZnFe_2O_4 samples were prepared by maintaining mixed powders of ZnO and Fe_2O_3 for 8 h at 800°C and then at 1200°C for another 8 h. Care was taken to use high purity starting materials in exact stoichiometric proportions. Sample 1 was slowly cooled (10 K/h) to room temperature, while sample 2 was rapidly quenched in a few seconds. The nanostructured sample 3 was produced by mechanical milling (75 h) [2] of an annealed powder sample. After milling an average particle size of about 9 nm was obtained. The three samples showed various degrees of inversion. For sample 1 no inversion was detected by neutron scattering within the limits of accuracy (3%). For sample 2 the degree of inversion had risen to 11%. For the nanostructured sample 3 it was 43%. As shall be seen, the three samples exhibit quite different magnetic behavior and it is highly suggestive that these differences are coupled, at least in part, to the rising degree of inversion.

μSR measurements were performed at the decay-channel muon beam μE1 and the surface muon beams πM3 at PSI and M13 at TRIUMF. Polycrystalline powder samples were used throughout. For the measurements at the decay-channel beam the powder was contained in a cylindrical silver can of 20 mm diameter and 21 mm height. For this sample geometry muon momenta between 70 and 82 MeV/c gave the best signal/background ratios. For the work using surface muon beams the powders were pressed into a flat disc-shaped pot of high purity Ag with 18 mm diameter and closed on the beam entrance side by a $5\mu\text{m}$ Mylar foil. Spectra were recorded from 2 to 320 K.

The neutron diffraction measurements used the time-of-flight diffractometer ROTAX at the pulsed spallation source ISIS, Rutherford Appleton Laboratory, UK. Complementary measurements were carried out on the conventional powder diffractometer SV7 at the FRJ-2 reactor of the Forschungszentrum Jülich. Diffraction patterns were collected in the temperature range from 2 to 300 K. Additional data (300–820 K) were obtained for sample 3 on ROTAX. All neutron measurements were performed on the sample material contained in cylindrical vanadium cans of 11 mm diameter

and 40 mm height. μSR measurements were carried out on the same material.

The ^{57}Fe Mössbauer effect measurements were recorded in transmission geometry using a conventional Mössbauer spectrometer with a $^{57}\text{CoRh}$ source. All samples were taken from the μSR batches.

3. Results and discussion

Information on the behavior of sample 1 is given in earlier publications [3,4] with Fig. 1 showing the magnetic phase diagram as derived mainly from μSR and neutron diffraction data. The Néel transition at 10.5 K was well established and was easily verified. However, the magnetic behavior turned out to be considerably more complex than a simple transition into an antiferromagnetic (AF) state. A magnetically short-range ordered (SRO) fraction first appears around 60 K. As shown in Fig. 1, this fraction increases significantly to $\sim 75\%$ on cooling to T_N , with the remaining fraction of the annealed sample, $\sim 25\%$, undergoing a transition to long-range AF order (LRO). On further cooling below T_N , the SRO fraction is found to decrease rapidly before reaching a saturation level of around 20%. This demonstrates that SRO and LRO magnetic states coexist in a normal Zn-ferrite for $T \rightarrow 0\text{ K}$. The exact spin structure of the AF LRO state is under some debate [5,6]. The position of the main broad SRO peak in the powder diffraction

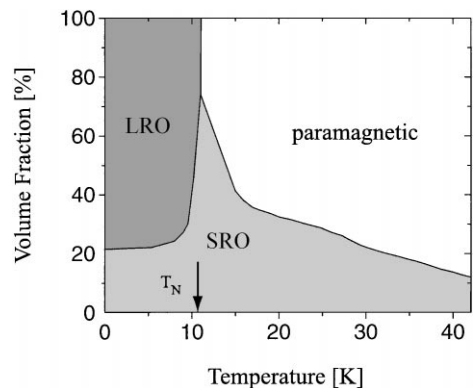


Fig. 1. Magnetic phase diagram of the annealed sample.

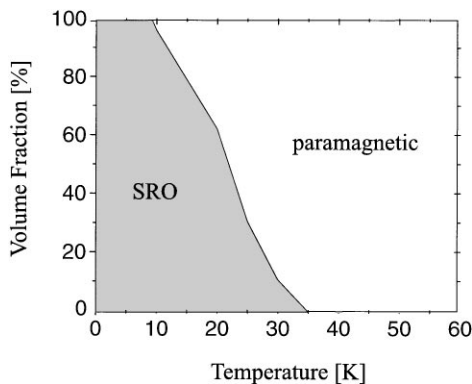


Fig. 2. Magnetic phase diagram of the quenched sample.

pattern differs only slightly from that of the LRO Bragg reflection. The AF structures might thus be quite similar, but the SRO correlation length (deduced from the reflection width) is only ~ 2.7 nm. Longitudinal field μ SR measurements prove that the SRO spin system retains fast spin dynamics. Fields of 0.3 T had no effect on either the paramagnetic or SRO relaxation rates.

Neutron diffraction could not detect LRO in sample 2. The combination with μ SR data leads to the phase diagram of Fig. 2. SRO is found to develop below 35 K, increasing in volume fraction to 100% at ~ 10 K – close to the Néel temperature of normal Zn-ferrite. The positions of the SRO peaks are similar to those of sample 1, although the peak widths were found to have increased considerably. The AF local correlations have not significantly changed, but the correlation length is further reduced to ~ 2 nm. Longitudinal field (B_{LF}) μ SR data again show that the SRO spin system is not frozen. Longitudinal fields up to ~ 0.3 T *do* affect the muon relaxation, in contrast to sample 1. Evaluation using the common expression for the relaxation rate in the fast fluctuation limit ($\lambda(B_{LF}) = \lambda(0)/[1 + \gamma_\mu^2 B_{LF}^2 \tau_c^2]$) yields fluctuation rates $1/\tau_c$ of the order of 10^8 Hz. This is less than the typical paramagnetic spin fluctuation rate (10^{10} Hz), which persisted in the SRO state of sample 1. Clearly the spin correlations have become enhanced in sample 2.

The magnetic behavior of the nanostructured sample 3 was even more interesting. One could

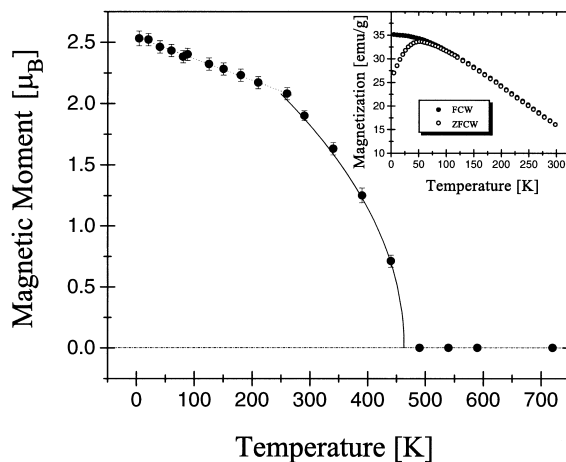


Fig. 3. Temperature dependence of the magnetic moment per iron atom for the nanostructured sample as derived from neutron diffraction. The inset shows the DC-magnetization data obtained on warming the sample after first cooling in both zero and applied (0.1 T) magnetic fields.

argue that a further increase of the degree of inversion would prevent any type of magnetic order. In contrast, neutron diffraction found ferromagnetic (FM) order commencing already at $T_c \approx 460$ K with an unusual, non-Brillouin-like temperature dependence of the effective magnetic moment (see Fig. 3) [7]. At a first glance, this behavior might indicate that only a (temperature dependent) portion of the compound undergoes ferromagnetic LRO. However, as will be shown below, the total sample exhibits ferromagnetic LRO.

No spontaneous oscillations were observed in the zero field μ SR spectra. The μ SR spectra can still be described by the typical response for LRO magnetism

$$A(t) = A_0 \left(\frac{2}{3} e^{-\lambda_\perp t} \cos(2\pi\nu_\mu t + \phi) + \frac{1}{3} e^{-\lambda_\parallel t} \right) \quad (1)$$

in the limit that $\lambda_\perp > \nu_\mu$. With $\lambda_\perp > 20 \mu\text{s}^{-1}$ this leads to $\nu_\mu < 10$ MHz corresponding to a local field $B_\mu < 0.1$ T. This provides insight to the local environment of muons in the nanostructured sample although the locations of the muon stopping sites are not yet known. We found that low applied fields ($B_{\text{appl}} \leq 30$ mT) do not enter the sample, in accordance with FM order. The fact that larger fields are able to penetrate the material suggests a

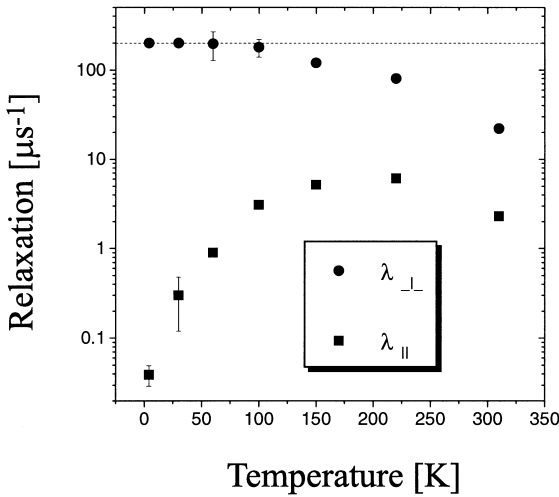


Fig. 4. Temperature dependence of the relaxation rates λ_{\perp} and λ_{\parallel} (see Eq. (1)) of the nanostructured sample.

ferromagnet of low saturation. Importantly, we find that the initial asymmetry A_0 is temperature independent (between 4 and 320 K) as expected for full response of the whole sample volume. No second fraction exists: all of the sample has entered the FM state at T_c . Spin dynamical processes, similar to those observed in RFe_6Al_6 (R = rare earth) compounds [8], are likely to account for the non-Brillouin-like shape of the temperature dependence of the effective magnetic moment shown in Fig. 3. Further insight to the sample behavior is contained in the two relaxation rates λ_{\perp} and λ_{\parallel} . The perpendicular rate responds to the static distribution *and* the fluctuations of the local field, while the longitudinal rate is sensitive to the dynamical field properties *only*. As shown in Fig. 4, $\lambda_{\perp} \gg \lambda_{\parallel}$ at all temperatures. This indicates that a field distribution (inhomogeneous line broadening) dominates. The increase in λ_{\perp} on cooling is due to the increase of the effective moment. Below 100 K the rate λ_{\parallel} drops sharply which reflects a freezing of fluctuations. This behavior fits in well with the Mössbauer spectra shown in Fig. 5. The spectra are characteristic for superparamagnetic materials approaching their blocking temperature [7]. The small particle size in sample 3 causes fluctuations of the resultant FM moment of each particle which probably consists of a single domain. When

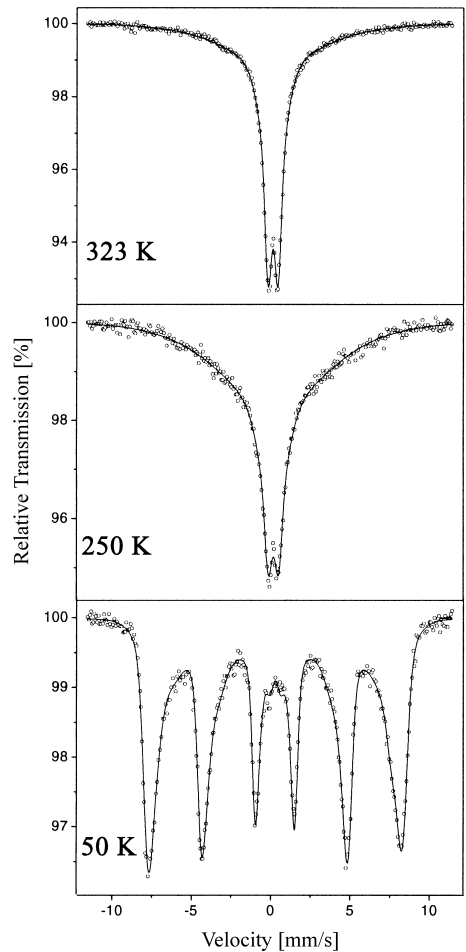


Fig. 5. ^{57}Fe Mössbauer spectra of the nanostructured sample at various temperatures.

freezing of the paramagnetic and local spin fluctuations (as reflected in λ_{\parallel}) has occurred around 50 K, the DC-magnetization data (inset to Fig. 3) show that the system attains a sensitive spin glass-like dependence on applied field conditions. The μSR data exhibit analogous effects: spin precession could be induced when the sample was field cooled through the spin freezing temperature. The spins become aligned in the magnetic field and maintain their preferred orientation when spin freezing sets in.

4. Conclusions

The normal Zn-ferrite shows the interesting but unexpected coexistence of LRO and SRO. Similar

behavior has also been observed by μ SR in the frustrated AF YMn_2 and related compounds [9,10]. The behavior of the quenched sample is typical for a highly frustrated system which cannot support LRO and deviates into spin glass-like magnetism [11]. This would mean that an originally present weak frustration in the AF couplings is enhanced by a higher degree of inversion. Enhanced spin correlations are also observed in sample 2 as a result of the relatively strong coupling between A and B sites. The still higher inversion in the nanostructured sample strengthens the A–B coupling even further, leading to strong magnetic interactions between the Fe ions and thus to FM spin couplings. The small size of the magnetic particles causes superparamagnetism in the single-domain nanocrystals. These fluctuations freeze at ~ 50 K. The magnetic behavior below this freezing temperature is strongly dependent on applied magnetic fields similar to that shown by spin glasses. Full details of the results and analyses will be published elsewhere [12].

Acknowledgements

Financial support by the Deutsche Forschungsgemeinschaft under Contract Nos. KA598/4-1

and KA598/4-2 and by the BMBF, Bonn, under Contract Nos. KI5BO2 and KI5BO3 is gratefully acknowledged. SJC and WAK acknowledge the support of the Australian Research Council.

References

- [1] R.E. Vandenberghe, E. De Grave, in: G.J. Long, F. Grandjean (Eds.), *Mössbauer Spectroscopy Applied to Inorganic Chemistry*, Vol. 3, Plenum, New York, 1989.
- [2] W.A. Kaczmarek et al., *IEEE Trans. Magn.* 30 (1994) 732.
- [3] W. Schiessl et al., *Phys. Rev. B* 53 (1996) 9143.
- [4] W. Potzel et al., *Hyperfine Interactions* 97/98 (1996) 373.
- [5] U. König et al., *Solid State Commun.* 8 (1970) 759.
- [6] U. König et al., *J. Phys. (Paris)* 32 (1971) C1.
- [7] W. Schäfer et al., *Mater. Sci. Forum* 321–324 (2000) 802.
- [8] G.M. Kalvius et al., *Physica B* 289–290 (2000), these proceedings.
- [9] S. Morup, H. Topsoe, *Appl. Phys.* 11 (1976) 63.
- [10] M. Weber et al., *Hyperfine Interactions* 85 (1994) 265.
- [11] B.D. Gaulin, *Hyperfine Interactions* 85 (1994) 159.
- [12] W. Potzel et al., *Hyperfine Interactions*, submitted.